

G. E. Elsinga · B. W. van Oudheusden · F. Scarano

Evaluation of aero-optical distortion effects in PIV

Received: 1 October 2004 / Revised: 15 February 2005 / Accepted: 21 April 2005 / Published online: 13 July 2005
© Springer-Verlag 2005

Abstract Aero-optical distortion effects on the accuracy of particle image velocimetry (PIV) are investigated. When the illuminated particles are observed through a medium that is optically inhomogeneous due to flow compressibility, the resulting particle image pattern is subjected to deformation and blur. In relation to PIV two forms of error can be identified: position error and velocity error. In this paper a model is presented that describes these errors and particle image blur in relation to the refractive index field of the flow. In the case of 2D flows the model equations can be simplified and, furthermore, the background oriented schlieren technique (BOS) can be applied as a means to assess and correct for the optical error in PIV. The model describing the optical distortion is validated by both computer simulation and real experiments of 2D flows. Two flow features are considered: one with optical distortion normal to the velocity (shear layer) and one with optical distortion in the direction of the flow (expansion fan). Both simulation and experiments demonstrate that the major source for the velocity error is the second derivative of the refractive index in the direction of the velocity vector. The aero-optical distortion effect is less critical for shearing interfaces in comparison with compression/expansion fronts, the most critical case being represented by shock waves. Based on the results from the simulated experiments, it is concluded that for the 2D flow case the BOS method allows a measurement of the mean velocity error in PIV and can reduce it to a large extent.

1 Introduction

Particle image velocimetry (PIV) is nowadays applicable to high-speed flows including the supersonic flow regime thanks to advances in high energy pulsed lasers and CCD technology (microsecond inter-framing time). However, since the first applications in transonic (Raffel and Kost 1998) and supersonic flows (Urban and Mungal 2001; Haertig et al. 2002) the problem of applying optically based techniques through inhomogeneous media was raised. More recent applications in the supersonic regime (Scarano and van Oudheusden 2003; Abart et al. 2004; Elsinga et al. 2004b), pointed out more clearly that the process of particle imaging in compressible flows can be far from trivial across shock waves and shear layers.

The present study investigates the effect of aero-optical distortion on the accuracy of optical flow velocimetry techniques. In particular planar particle imaging techniques, such as PTV and PIV, are considered. These methods track particle image motion in a planar domain within the flow field. Distortion of the imaging process occurs if the illuminated particles are observed through an optically inhomogeneous medium, as in the case of compressible flows or thermal convection flows. The resulting image of the particle image pattern is subjected to deformation and individual particles may be perceived as blurred. In relation to particle imaging velocimetry two forms of error can be identified: position error and velocity error.

The position and velocity error are a direct consequence of the geometrical deformation of the image, which results in a systematic (bias) error of the measured velocity. In synthesis one may say that the wrong velocity vector is evaluated at the wrong position. Image blur affects the tracking precision in terms of cross-correlation accuracy due to the (anisotropic) increase of the particle image size, thus broadening the correlation peak. In the following discussion, the emphasis is given to the characterisation of the first two types of errors.

G. E. Elsinga (✉) · B. W. van Oudheusden · F. Scarano
Department of Aerospace Engineering,
Delft University of Technology, Kluyverweg 1,
2629 HS Delft, The Netherlands
E-mail: g.e.elsinga@lr.tudelft.nl
Tel.: +31-15-2786386

The image distortion is put in relation to the refractive index spatial distribution. From this optical model, an analytical expression for the position error is derived. Subsequently, the velocity error is obtained from spatial differentiation of the position error. The scale-up of the optical distortion effects to a compressible flow experiment in high-speed industrial wind tunnels is briefly discussed in the [Appendix](#).

The second objective of the present study is to indicate a strategy to diagnose the aero-optical effects from real experiments and possibly correct for them. Given the similarity of the phenomenon of aero-optical distortion with the measurement principle of background oriented schlieren (BOS), this technique is chosen to perform the experimental verification of aero-optical distortion in a 2D flow. The BOS is nowadays a relatively accessible technique when PIV hardware is available in research laboratories. It can therefore be seen as a complementary technique with respect to PIV. The operating principle of the BOS method relies on optical distortion of a background pattern to visualise the refractive index field (Richard and Raffel 2001) and is therefore of direct relevance to the present problem. Moreover, the measurement accuracy of the technique has been now established even in comparison with calibrated colour schlieren and PIV (Elsinga et al. 2004a).

The model describing the PIV error is verified by means of BOS with a 2D flow experiment and a computer simulation based on light ray tracing. Two types of flow are considered: one with optical distortion normal to the flow velocity (shear layer) and one with optical distortion in the direction of the flow velocity (1D expansion), which represent schematically the situation encountered in the experimental condition when a separated shear layer and Prandtl-Meyer expansion fan are observed over a 2D wind tunnel model.

2 Optical distortion in PIV

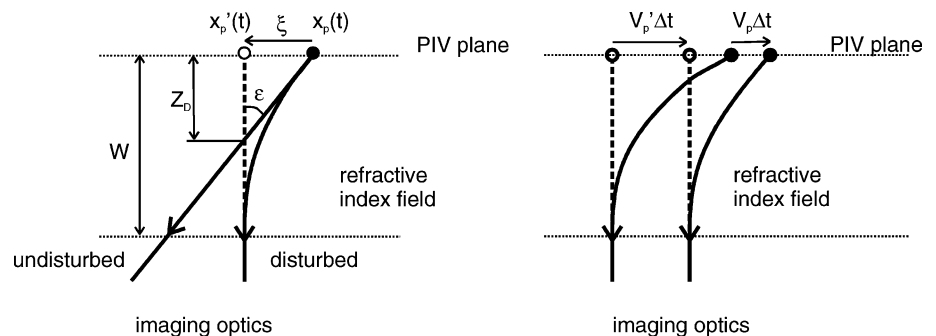
In this section, the error introduced in PIV by optical distortion is modelled on the bases of geometrical optics. The position and velocity error are assessed in relation to the refractive index field between the PIV measurement plane and the imaging optics. Finally evidence of

severe imaging distortion is discussed with an example of particle image blur across a shock wave.

The problem is discussed in the hypothesis of steady flow for simplicity. This hypothesis can easily be removed generalizing the validity of the results to unsteady flows. The particle velocity \overline{V}_p and the image distortion, which is related to the flow density field, depend only on the spatial location in the imaging plane. In order to separate the effects of different sources of error, the present model assumes ideal imaging and tracking conditions, i.e. pixelisation effects are neglected and the time separation between exposures is assumed small enough to neglect the time averaging error on the velocity. Furthermore, the averaging effect of the finite interrogation window size is neglected as well. In the present analysis the velocity considered is that of the particle, keeping in mind that this may differ from the actual local flow velocity due to particle lag. The particle-image density is assumed to be sufficiently high (high image number density) to allow the continuous measurement of the velocity field.

Because of the one-to-one relation between the recording plane and the plane of focus, the recorded PIV image can be thought of as being formed in the plane of focus. As a consequence, the magnification factor of the imaging system can be ignored. After a light ray coming from a particle in the PIV measurement plane has left the refractive index field in the test section, it propagates along a straight line. A linear backward extension of that line to the plane of focus provides the position at which that particle is perceived by the imaging system (Fig. 1). For simplicity, it is assumed in the figures that the imaging system only collects light rays leaving the refractive index field parallel to the optical axis, this limitation not being essential for the description of the optical errors. Figure 1 (left) shows an undisturbed light ray propagating through a homogeneous refractive index field and the disturbed one (through an inhomogeneous refractive index field) coming from a single particle and initially propagating in the same direction. A backward extension of the two light rays (dashed line) reveals that for the disturbed light ray, the imaged position of the particle (open circle) is different from the actual position of the particle in the PIV plane (solid circle). This spatial displacement is referred to as the position error. Figure 1 (right) shows a single

Fig. 1 Optical distortion in PIV: position error (left) and direct velocity error (right). Solid lines represent light ray trajectories coming from the particle (solid circle). Dashed lines are the backward extension of those rays indicating the position where the particle is perceived in the PIV plane (open circles)



particle (moving to the right) at two subsequent exposures separated by a time interval Δt . The position error at the two spatial locations may differ returning different position errors for the two particle images. This results in an error in the particle image particle displacement, hence measured particle velocity. This is referred to as the direct velocity error.

2.1 Particle position error

Let the image distortion be expressed in terms of an optical displacement vector $\vec{\xi}(\vec{x})$, as:

$$\vec{\xi}(\vec{x}_P(t)) = \vec{x}_P'(t) - \vec{x}_P(t) \quad (1)$$

where $\vec{x}_P(t)$ is the actual particle location (x, y) in the measurement plane and $\vec{x}_P'(t)$ is the location where that particle is perceived (Fig. 1 left). The optical displacement vector is directly equivalent to the position error of the measurement and is related to the gradient of the refractive index ∇n . The BOS studies (Richard and Raffel 2001; Elsinga et al. 2004a) propose the following expression for the optical displacement vector based on the theory of light propagation in a refractive index field (using $n \sim 1$):

$$\vec{\xi}(\vec{x}) = -Z_D \vec{\epsilon}(\vec{x}) = -Z_D \int_s \nabla n(\vec{x}, z) dz \quad (2)$$

where z is the coordinate direction normal to the PIV measurement plane, ϵ the light beam deflection angle and Z_D is the distance parallel to the optical axis between the measurement plane and the intersection point of the disturbed ($\nabla n \neq 0$) and undisturbed ($\nabla n = 0$) light rays coming from the same particle (Fig. 1 left). The refractive index n depends on the density ρ according to the Gladstone–Dale relation, i.e. $n = 1 + K\rho$ where $K = 2.3 \times 10^{-4} \text{ m}^3/\text{kg}$ for air.

2.2 Velocity error

Following a Lagrangian approach to the tracking of a particle (image), the particle velocity \vec{V}_P is related to the particle displacement in time as:

$$\vec{V}_P(\vec{x}_P(t)) = \frac{d\vec{x}_P(t)}{dt} \quad (3)$$

In PIV the time interval between the two exposures is finite, which may introduce a difference between the instantaneous and the measured velocity (time averaging), which is neglected in the present discussion. The observed or measured particle velocity \vec{V}_P' , obtained from the optically distorted images, is then given by

$$\vec{V}_P'(\vec{x}_P'(t)) = \frac{d\vec{x}_P'(t)}{dt} \quad (4)$$

The velocity error of the measurement is now defined as the difference between the measured velocity and the actual particle velocity at a given location \vec{x} in the image:

$$\begin{aligned} \Delta \vec{V}_P(\vec{x}) &= \vec{V}_P'(\vec{x}) - \vec{V}_P(\vec{x}) = \left\{ \vec{V}_P'(\vec{x}_P'(t)) - \vec{V}_P(\vec{x}_P(t)) \right\} \\ &\quad + \left\{ \vec{V}_P(\vec{x}_P(t)) - \vec{V}_P(\vec{x}_P'(t)) \right\} \\ &= \left\{ \frac{d\vec{x}_P'(t)}{dt} - \frac{d\vec{x}_P(t)}{dt} \right\} + \frac{\partial \vec{V}_P}{\partial \vec{x}} (\vec{x}_P(t) - \vec{x}_P'(t)) \end{aligned} \quad (5)$$

Substitution of the optical displacement vector (Eq. 1) and further evaluation yields:

$$\begin{aligned} \Delta \vec{V}_P(\vec{x}) &= \frac{d\vec{\xi}(\vec{x}(t))}{dt} - \frac{\partial \vec{V}_P}{\partial \vec{x}} \vec{\xi}(\vec{x}) = \frac{\partial \vec{\xi}}{\partial \vec{x}} \vec{V}_P(\vec{x}) - \frac{\partial \vec{V}_P}{\partial \vec{x}} \vec{\xi}(\vec{x}) \\ &= \left(\nabla \vec{\xi} \right) \vec{V}_P - \left(\nabla \vec{V}_P \right) \vec{\xi} \end{aligned} \quad (6)$$

The first term represents the direct velocity error (Fig. 1 right), which is given by the product of the actual particle velocity and the gradient of the optical displacement vector. The latter represents a local change in optical magnification, which “stretches” the imaged object with respect to the physical dimension in the measurement plane. The second term in Eq. 6 is the product of the optical displacement vector with the gradient of the actual particle velocity and represents the contribution of the position error to the velocity error. It has been assumed in the analysis that in first approximation $\nabla \vec{\xi}$ is constant over the particle displacement between the recordings and that the velocity gradient is constant along the optical displacement $\vec{\xi}$ (first order Taylor expansion). Note that only the derivative of the optical displacement vector taken in the direction of the velocity vector contributes to the first term of the velocity error. It was shown previously that the optical displacement vector is related to the gradient of the refractive index (Eq. 2).

Under certain conditions the optical displacement vector field $\vec{\xi}$ can be measured independently using the BOS technique. In that case the measured velocity \vec{V}_P' can be corrected using the expression for the velocity error (Eq. 6) to obtain the exact particle velocity \vec{V}_P , as will be explained in Sect. 3.

2.3 Particle image blur

According to the principle described in Fig. 2 the optical distortion can introduce a blurring effect on the imaging of individual particle images. The scattered light from a particle is captured by the imaging optics through a finite solid angle of semi-aperture θ . When changes in the amount of deflection occur within the mentioned

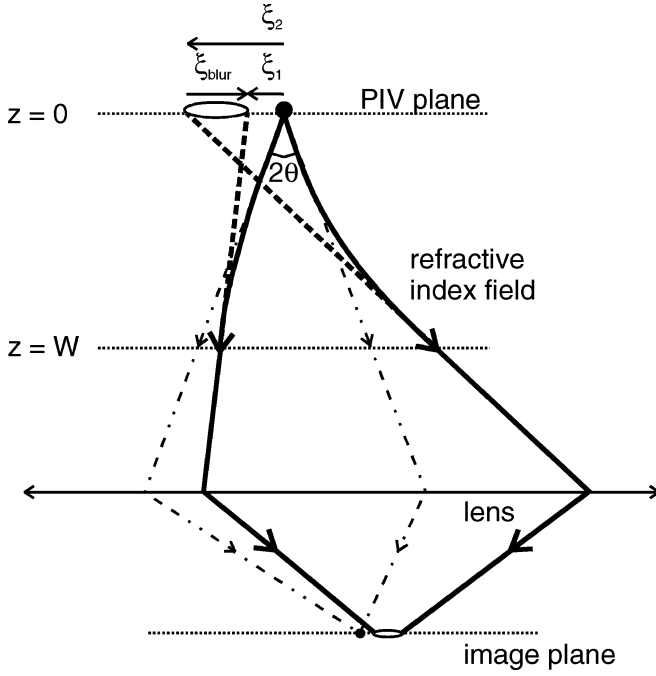


Fig. 2 Principle of refractive particle image blur. *Solid lines* represent light ray trajectories coming from the particle (*solid circle*) edges in an inhomogeneous refractive index field. *Dashed lines* are the backward extension of those rays indicating the edges where the particle appears in the PIV recordings (*open ellipse*)

angle (due to a local variation in the gradient of refractive index), the imaging system becomes astigmatic producing a blurred particle image. In this case the second derivative of the refractive index is the driving term for the error and cannot be neglected. A re-evaluation of the optical displacement in the x -direction yields:

$$\begin{aligned} \xi &= \Delta x_{z=W} - W \Delta x'_{z=W} = \int_0^W \Delta x' dz - W \int_0^W \frac{\partial n}{\partial x} dz \\ &= \int_0^W \int_0^z \frac{\partial n}{\partial x} dz dz - W \int_0^W \frac{\partial n}{\partial x} dz \end{aligned} \quad (7)$$

where Δx is the deviation along the x coordinate and $\Delta x'$ is the change in direction (dx/dz) from the undisturbed light ray. W is the length of the light path through the refractive index field in the z direction (for PIV application in a supersonic wind tunnel it is the distance between the measurement plane and the tunnel window). In the assumption of small Δx , $\Delta x'$ and angle θ , the gradient of refractive index along the two light rays is given by:

$$\frac{\partial n}{\partial x_{1,2}} = \frac{\partial n}{\partial x_{\text{ref}}} \mp \frac{\partial^2 n}{\partial x^2} \theta z \quad (8)$$

where $\frac{\partial n}{\partial x_{\text{ref}}}$ and $\frac{\partial^2 n}{\partial x^2}$ are allowed to vary with z . Consequently the particle is imaged on a stretched area of length ξ_{blur} , which is given by:

$$\begin{aligned} \xi_{\text{blur}} &= \xi_1 - \xi_2 = \int_0^W \int_0^z -2 \frac{\partial^2 n}{\partial x^2} \theta z dz dz + W \int_0^W 2 \frac{\partial^2 n}{\partial x^2} \theta z dz \\ &\sim \theta W^3 \end{aligned} \quad (9)$$

This expression considers only refractive blur based on geometrical optics. Diffractive effects can be accounted for by a convolution of the geometric particle image (stretched) and the diffraction spot (circular). From Eq. 9 it is seen that the amount of blur depends on θ , which in turn depends on the aperture or $f/\#$ of the imaging optics. Increasing $f/\#$ reduces (geometrical) particle image blur by reducing the solid angle of the captured light cone hence the region of the flow influencing the imaging of the particle. This conclusion is supported by the analysis of blur in BOS images made by Sourgen et al. (2004), but remains to be validated with experiments. Unfortunately, increasing $f/\#$ has limited applicability since the perceived particle peak intensity is inversely proportional to $f/\#^4$. Furthermore, the expression for ξ_{blur} is non-linear in z , so that the influence of the refractive index field on the blurring increases with the distance to the measurement plane z .

Particle image blur is typically encountered when imaging across flow features that act as optical interfaces such as shock waves, shear layers and boundary layers, due to a large value of the spatial second derivative of the refractive index field. Also a flow expansion (e.g. Prandtl-Meyer expansion fan) may cause particle image blur in some experimental conditions. An example of particle image blur is given in Fig. 3, which shows a PIV recording of a planar oblique shock wave (left) and the measured velocity field (right). Details of the image at locations (A) and (B) are presented in Fig. 4. In the uniform flow region (A) the refractive index is also uniform; therefore, the light scattered by the tracer particles is transmitted without distortion and no blur is observed. At location (B), representing the shock wave, the particle image is blurred in the direction normal to the shock as expected due to the local variation of the refractive index. It is seen in Fig. 4 that the particle peak brightness has decreased as a result of blur. An estimate for the maximum enlargement ξ_{blur} in the measurement plane near a shock wave, based on Snell's law, is given by (Raffel and Kost 1998):

$$\xi_{\text{blur}} = W \sqrt{2 \Delta n} \quad (10)$$

where Δn is the refractive index difference across the shock. The factor $\sqrt{2 \Delta n}$ is the maximum light deflection angle caused by the shock. Equation 10 would return for the present case $\xi_{\text{blur}} = 1.6$ mm corresponding to approximately 60 pixels. This is an overestimation judging from a qualitative inspection of Fig. 4 ($\xi_{\text{blur}} \sim 20$ pixels). The main drawback of particle image blur is the consequent reduction in particle image contrast and correlation signal-to-noise ratio. When comparing the

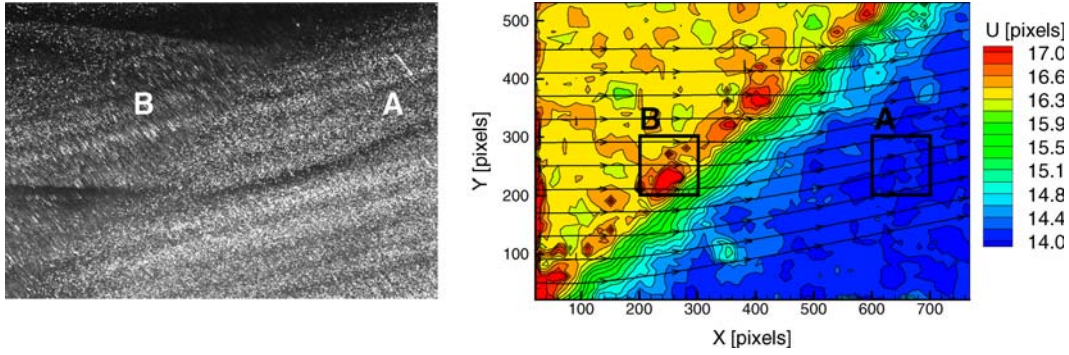


Fig. 3 PIV recording of a 2D oblique shock wave at $M=2$ (left) and the resulting u -component of velocity in pixel units with streamlines (right)

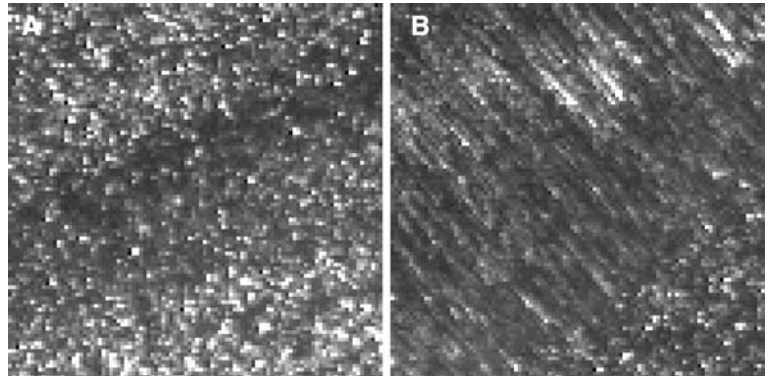
cross-correlation results for (A) and (B), it is found that at the location with particle image blur (B) the measurement noise has increased. This is explained by the correlation peak broadening with a consequent drop in the signal to noise ratio and cross-correlation accuracy.

3 Two-dimensional flow hypotheses

The theory described so far will be verified by means of experiments and a numerical simulation. The experimental verification makes use of BOS as a technique to measure the optical distortion. In order to proceed with a quantitative assessment two-dimensional test cases are selected. Moreover the 2D case allows simplifying the model equations for optical distortion significantly. In the assumption that the gradient of refractive index is independent of z (2D flow) the light ray trajectory is approximated by a parabola, in which case Z_D can be taken as $W/2$ (Elsinga et al. 2004a). The expression for the optical displacement vector (Eq. 2) then reduces to:

$$\vec{\xi}(\vec{x}) = -Z_D \int_0^W \nabla n(\vec{x}) dz = -Z_D W \nabla n(\vec{x}) = -\frac{1}{2} W^2 \nabla n(\vec{x}) \quad (11)$$

Fig. 4 Detail (100×100 pixels) of the PIV recording of Fig. 3 at positions A and B



Using this result, the gradient of the optical displacement vector in Eq. 6 is given by:

$$\nabla \vec{\xi}(\vec{x}) = -\frac{1}{2} W^2 \frac{\partial \nabla n(\vec{x})}{\partial \vec{x}} = -\frac{1}{2} W^2 \nabla^2 n(\vec{x}) \quad (12)$$

3.1 Verifying optical distortion theory using BOS

The BOS method exploits the optical distortion effects to visualise the refractive index field (Raffel et al. 2000; Richard and Raffel 2001; Klinge and Riethmuller 2002). In some cases BOS can be used to quantitatively determine the density field (or refractive index field) as shown by Elsinga et al. (2004a). In terms of image processing procedures, the BOS technique is very similar to PIV. It employs a computer generated PIV image, which in the present study is placed at the backside of the test section. The background pattern is imaged with a CCD camera before and during the experiment. Thus, two images of the background pattern are taken and the relative displacement caused by the difference in the refractive index field is measured by means of cross-correlation, similar to what is performed in PIV.

Performing a PIV experiment through a spatially varying refractive medium both recordings are distorted, and the particle displacement cannot be distinguished from the optical distortion. For BOS, the undistorted pattern is known from a recording of the background without flow in the test section

(homogeneous refractive index). The displacement field measured independently with BOS can be employed to assess and, in the case of 2D flow, to correct the optical distortion effect in the PIV measurements. However, the BOS displacement vector is obtained with the particle image pattern placed on the opposite side of the wind tunnel and represents the integral effect of optical distortion across the test section, whereas the PIV measurement plane is located inside the flow, often in the mid-section. This means that the gradient of refractive index is integrated over different paths, W_{BOS} and W_{PIV} ; therefore, the BOS displacement vector requires a proper scaling before it can be applied to correct PIV measurements. A scaling factor can be determined assuming that the light rays collected by the imaging optics are parallel to the optical axis for both BOS and PIV, so that the field of view of BOS does not need to be scaled to the field of view in the PIV measurement plane (Klinge and Riethmuller 2002). This condition can be asymptotically reached by placing the imaging optics at a large distance from the object. Under the restrictive assumption that the gradient of refractive index is independent of z (2D flow), the optical displacement vector due to the refractive index field in BOS ($\vec{\xi}_{\text{BOS}}$) and PIV ($\vec{\xi}_{\text{PIV}}$) are expressed by:

$$\begin{aligned}\vec{\xi}_{\text{BOS}}(\vec{x}) &= -(Z_{\text{D}}W)_{\text{BOS}}\nabla n(\vec{x}) \\ \vec{\xi}_{\text{PIV}}(\vec{x}) &= -(Z_{\text{D}}W)_{\text{PIV}}\nabla n(\vec{x})\end{aligned}\quad (13)$$

Elimination of the gradient of the refractive index yields:

$$\vec{\xi}_{\text{PIV}}(\vec{x}) = \frac{(Z_{\text{D}}W)_{\text{PIV}}}{(Z_{\text{D}}W)_{\text{BOS}}}\vec{\xi}_{\text{BOS}}(\vec{x}) = A\vec{\xi}_{\text{BOS}}(\vec{x})\quad (14)$$

using $Z_{\text{D}}=W/2$, the scaling factor $A=W_{\text{PIV}}^2/W_{\text{BOS}}^2=0.25$, with the PIV measurement plane located at the centre of the test section ($W_{\text{PIV}}=W_{\text{BOS}}/2$). Using $\vec{\xi}_{\text{PIV}}$ with Eq. 1 and the first right-hand-side term of Eq. 6 for the direct velocity error (the second term has the same effect as using Eq. 1 to correct for the measurement position), the PIV measurement can be corrected for optical distortion by applying:

$$\begin{aligned}\vec{x}_{\text{Pcorr}} &= \vec{x}_{\text{P}}' - \vec{\xi}_{\text{PIV}} \\ \vec{V}_{\text{Pcorr}}(\vec{x}_{\text{Pcorr}}) &= \left(I + \nabla\vec{\xi}_{\text{PIV}}\right)^{-1} \vec{V}_{\text{P}}'(\vec{x}_{\text{Pcorr}})\end{aligned}\quad (15)$$

where I is the identity matrix.

For more complex flow configurations (3D) finding the scaling rule is not a single parameter and the problem is associated to determine the 3D field distribution of the gradient of refractive index. For axi-symmetric flows Watt et al. (2000) and Sourgen et al. (2004) have shown that the refractive index variation can be obtained from conventional schlieren and BOS, respectively. In that case it is possible to calculate the optical distortion using Eqs. 2 and 6.

4 Numerical simulation

The model for the position and velocity error due to optical distortion, as presented in a previous section, is evaluated with numerical simulation of PIV experiments in the presence of a 2D refractive index field. Particle tracers behaviour, flow properties, illumination and imaging conditions are simulated taking as a reference actual experimental conditions in the transonic-supersonic wind tunnel (TST-27) at the Aerodynamics Laboratories of the Delft University of Technology. Seeding particles with a relaxation time $\tau_p=2.4\ \mu\text{s}$ are traced through a 2D flow field. The optical distortion is calculated using a light ray-tracing algorithm in the refractive index field. Using the results from particle and ray traces, synthetic PIV recordings are produced, which are analysed using a cross-correlation algorithm (window deformation iterative multi-grid scheme, WIDIM) with interrogation windows of 31×31 pixels and 50% overlap (Scarano and Riethmuller 2000). The PIV recordings are separated in time by $1\ \mu\text{s}$. Furthermore, synthetic BOS images are generated in order to verify the effectiveness of the BOS correction method for 2D flows. The dimensions of the test section and setup are $W_{\text{PIV}}=140\ \text{mm}$, $W_{\text{BOS}}=280\ \text{mm}$, $Z_{\text{D_PIV}}=W_{\text{PIV}}/2$ and $Z_{\text{D_BOS}}=164\ \text{mm}$ (the background pattern is mounted outside the tunnel onto the rear glass window). Consequently, the scaling factor A is equal to 0.21.

Two types of uni-directional flow ($v=0$) are considered: a constant thickness shear layer and a 1D expansion front. These are simplified models of realistic compressible flow features, such as a spatially developing free shear layer and an expansion fan, which will be considered in the experimental verification (Sect. 5). The simplifications allow identifying the effects of the position error and the direct velocity error separately.

4.1 Compressible shear layer

The variation of the flow velocity u across a shear layer is modeled as:

$$u(y) = u_0 + \Delta u \tan h\left(\frac{y}{\delta_0}\right); \quad \delta_0 = \frac{\Delta u}{\left(\frac{du}{dy}\right)_{y=0}}\quad (16)$$

where $\Delta u=250\ \text{m/s}$, $u_0=250\ \text{m/s}$ and $\delta_0=3\ \text{mm}$ is the thickness parameter. The velocity above and below the shear layer is 500 and 0 m/s, respectively. Since the flow acceleration is zero the tracer particles travel exactly at the flow velocity (no particle lag). Given a density of $0.90\ \text{kg/m}^3$ above the shear layer and assuming constant total temperature (290 K) and pressure across the shear layer, the density below the shear layer is $0.51\ \text{kg/m}^3$. The refractive index field is obtained using the Gladstone–Dale relation. Since the refractive index is a

function of the y -coordinate only, the gradient of the optical displacement vector (oriented in y direction, Eq. 12) is perpendicular to the velocity vector (oriented in x direction). Therefore the first term of the velocity error (direct velocity error, Eq. 6) cancels out and only the position error remains. Substituting Eq. 11 and the Gladstone–Dale relation, the resulting velocity error for the shear layer is given by:

$$\Delta u(y) = -\frac{\partial u(y)}{\partial y} \xi_y(y) = \frac{W^2}{2} K \frac{\partial \rho(y)}{\partial y} \frac{\partial u(y)}{\partial y} \quad (17)$$

where ξ_y is the y -component of the optical displacement vector.

Figure 5 shows the velocity profile across the shear layer. The qualitative agreement between measured and flow velocity is very good and the error due to the refractive index fields can be appreciated only with a close-up (Fig. 5 right). The estimate of the velocity error, Eq. 17, has been added to the particle velocity (triangles) to compare the distortion model with the measured velocity profile obtained from the synthetic images based on actual ray-tracing (squares). It is seen that the model accurately predicts the error in the measurement. The measured position error is 0.094 mm or 1.9 pixels and is not detectable on the scale of the field of view (50 mm). Due to the large velocity gradient in the shear layer the velocity error at $y=0$ is more significant at 7.9 m/s. A BOS correction would allow reducing the error to a small fraction of it (0.6 m/s corresponding to 0.01 pixel particle displacement).

Varying the thickness of the shear layer δ_0 does not yield significantly different results. The range of δ_0 on which the optical distortion model and the BOS correction method are effective is limited on one end by insufficient resolution for cross-correlation resulting in amplitude modulation (e.g. for $\delta_0=1$ mm cross-correlation errors dominate) and on the other end by the cross-correlation accuracy (e.g. for $\delta_0=5$ mm the error

associated with optical distortion is smaller than the cross-correlation accuracy).

4.2 One-dimensional gradual expansion front

An isentropic expansion is simulated in a simplified manner by means of a 1D gradual expansion front, for which the variation of the flow velocity u in the horizontal direction is taken as:

$$u(x) = u_0 + \Delta u \tan h \left(\frac{x}{\delta_0} \right) \quad (18)$$

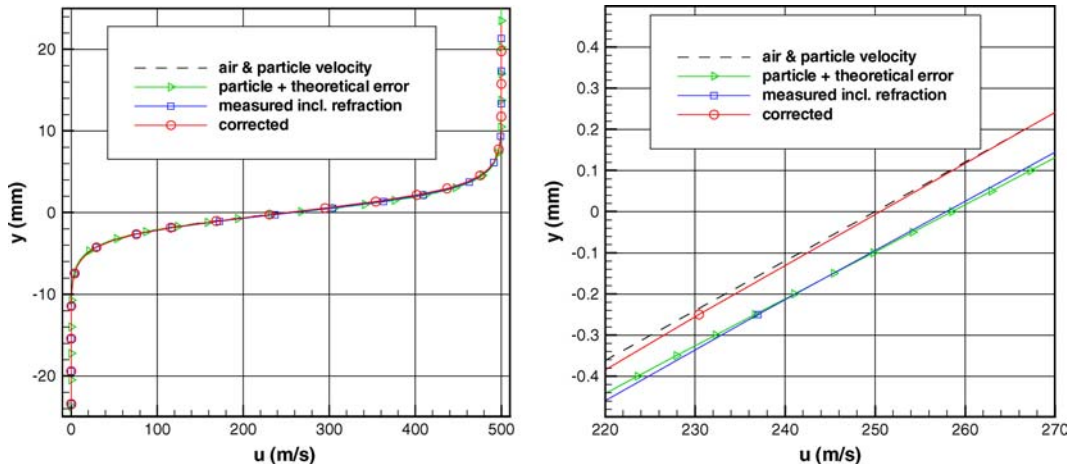
where $\Delta u=35$ m/s, $u_0=465$ m/s and $\delta_0=3$ mm. The velocity before and behind the expansion is 430 and 500 m/s, respectively. Given a density of 0.90 kg/m³ before the expansion, a total temperature of 290 K and using isentropic flow relations, the density behind the expansion is 0.58 kg/m³. In this case, the refractive index is a function of x only. Therefore the gradient of the optical displacement vector (Eq. 12) is oriented in the direction of the velocity vector (x direction) and both position and direct velocity errors are expected to affect the measurement. The velocity error for the 1D expansion is given by:

$$\begin{aligned} \Delta u(x) &= \frac{\partial \xi_x(x)}{\partial x} u(x) - \frac{\partial u(x)}{\partial x} \xi_x(x) \\ &= \frac{W^2}{2} K \left[-\frac{\partial^2 \rho(x)}{\partial x^2} u(x) + \frac{\partial \rho(x)}{\partial x} \frac{\partial u(x)}{\partial x} \right] \end{aligned} \quad (19)$$

where ξ_x is the x -component of the optical displacement vector. The second term of the velocity error is similar to the velocity error for the shear layer (Eq. 17).

Figure 6 shows the velocity profile across the expansion. Particle lag is clearly seen as a shift of the profile in the flow direction of about 1 mm leading to a velocity error of -10 m/s at $x=0$ mm. Since the flow velocity cannot be measured more accurately than as that of the particle, the error due to optical distortion is defined with respect to the particle velocity. As also observed for the shear layer, the velocity profile expected from Eq. 19 (triangles) agrees well with the measured

Fig. 5 Velocity profiles across the shear layer (*left*) and detail (*right*) with $\delta_0=3$ mm



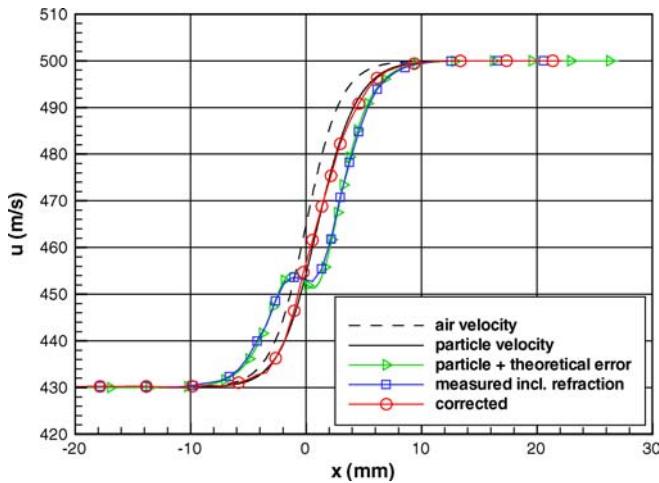


Fig. 6 Velocity profiles across the 1D expansion with $\delta_0 = 3$ mm

velocity returned from the synthetic images (squares), which further validates the optical distortion model. The magnitude of the velocity error is reduced in the measurement by amplitude modulation in the cross-correlation; therefore, even better agreement is found for smaller optical distortion (Fig. 7).

The refractive index field has a large effect on the measured velocity profile, as seen from Fig. 6. Not only is a velocity error introduced, but also the shape of the velocity profile has changed dramatically, which may lead to a misinterpretation of the flow. The most important source of error is the first term in Eq. 6, which represents the non-homogeneous stretching of the image length scales with respect to the physical length scales in the PIV measurement plane due to the gradient of the optical displacement vector. As also seen from the results of the shear layer, the error directly related to the optical displacement vector (i.e. the ‘position error’) does not result in a significant change in the shape of the velocity profile. In conclusion, even though the shear

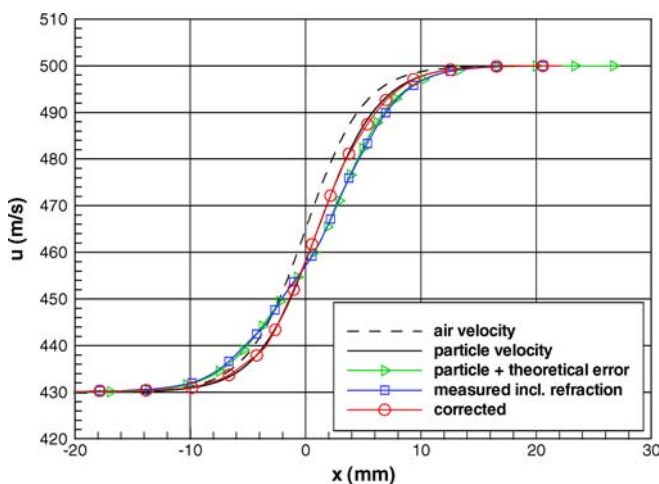


Fig. 7 Velocity profiles across the 1D expansion with $\delta_0 = 5$ mm

layer and the expansion have approximately the same thickness and density level, the velocity errors are very different due to the different orientation of the optical distortion with respect to the velocity vector, leading to the absence or presence of the direct velocity error.

The maximum error in position found for the expansion is 0.12 mm (2.4 pixels). The largest error in velocity is -14 m/s (found at $x = 2$ mm), which is mostly due to the gradient of the optical displacement vector (95%). Using the BOS correction would practically bring the error below the typical PIV uncertainty (0.1 pixel particle displacement).

Increasing the expansion thickness δ_0 to 5 mm, thereby reducing the optical distortion effects, results in a less pronounced change in the shape of the measured velocity profile (Fig. 7), i.e. the wiggle as seen in Fig. 6 has disappeared. However, the velocity gradient is clearly underestimated by PIV. From Fig. 7 it is again seen that BOS can be used effectively to correct for optical distortion. Concerning the range of δ_0 on which the optical distortion model and the BOS correction method are effective, the same considerations hold as for the shear layer.

5 Experimental verification

In this section experimental evidence of the velocity error due to optical distortion in compressible flow is given. In absence of the actual particle velocity data the errors are evaluated and corrected using the BOS method. The results are compared with the trends seen in the simulations.

The flow around the 2D wedge-plate model (Scarano and van Oudheusden 2003) is measured in the TST-27 supersonic wind tunnel at $M_{\infty} = 1.96$ and $P_0 = 1.97$ bars. The model spans the width of the test section (280 mm) and consists of a wedge with sharp leading edge imposing a flow deflection of 11.31° , followed by a plate 50 mm long and 20 mm thick. For the experimental investigation only the expansion fan located at the model shoulder and the shear layer are considered. The experimental parameters are the same as for the simulation (Sect. 4).

Although the model is 2D, some three-dimensionality in the flow is expected on the sidewalls (tunnel windows), e.g. expansion-boundary layer interaction. At the largest distance from the measurement plane the effect of density on optical distortion is largest. However, the spatial extent of these features is small compared to the width of the model and their effect will be neglected.

In the PIV and BOS experiments the light collected by the imaging optics is not parallel as in the case of the simulations. This means that the density gradient is not strictly constant along the optical path everywhere in the field of view. However, in the centre of the field of view the viewing angle with respect to the optical axis is relatively small. Furthermore, in non-parallel imaging

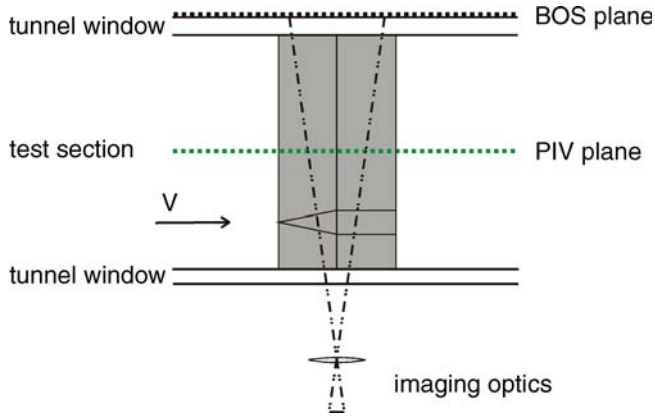


Fig. 8 Schematic of the PIV and BOS experimental arrangement (top view)

the BOS field of view, in general, needs to be scaled to the field of view in the PIV measurement plane (Klinge and Riethmuller 2002). Between PIV and BOS measurements the camera position remains fixed and only the focus is changed to a different plane (Fig. 8). This way the field of view in the PIV measurement plane, which is $55 \times 44 \text{ mm}^2$ for all experiments, does not change, so no scaling is required. A 1280×1024 pixels 12-bit CCD camera equipped with a Nikon 60 mm objective is used to record the images.

5.1 Shear layer

The left side of Fig. 9 shows the mean of the horizontal velocity component (averaged over 160 instantaneous velocity fields). In order to compare the measurement results with the simulation, the velocity component parallel to the shear layer axis V_s (in the direction of s ,

Fig. 9 Measured u -component of velocity in the base region of the 2D wedge-plate model (left), and profiles of the measured and corrected flow velocity V_s (right)

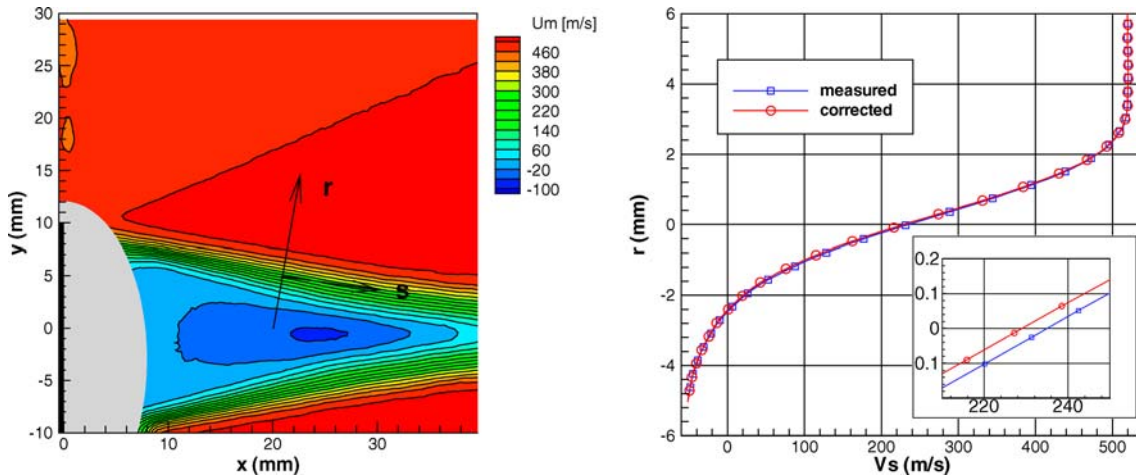


Fig. 9, left) is evaluated. In the direction normal to the shear layer (in the direction of r , Fig. 9 left) the velocity component is negligible. The right hand side of Fig. 9 presents a profile of V_s along r . The velocity across the shear layer ranges from 520 m/s to -50 m/s . Assuming constant pressure and total temperature across the shear layer, the density above and below the shear layer is estimated at 0.61 and 0.31 kg/m^3 , respectively. As suggested from the simulation of the shear layer (Sect. 4.1), the measurement overestimates the local velocity. At $r=0$ the BOS measurement predicts a velocity error of 5.8 m/s (corresponding to 0.14 pixel particle displacement) with a position error of 0.040 mm , for which the measurement is corrected (Fig. 9, right). The magnitude of the correction agrees well with the simulation results taking into account that the overall density level in the measurement, hence density gradient, is 67% of that used in the simulation.

5.2 Prandtl–Meyer expansion fan

The measurement result for the expansion fan located at the model shoulder is shown in Fig. 10 left. The average velocity field is obtained from 165 instantaneous fields. For a better comparison with the simulation of a one-dimensional expansion (Sect. 4.2), the velocity component in the direction of the density gradient V_s (in the direction of s , Fig. 10 left) is considered here. Figure 10 (right) presents the variation of V_s with s . V_s increases from 232 to 335 m/s across the expansion. The density before and after the expansion is estimated at 0.92 and 0.61 kg/m^3 , respectively. The measured and BOS corrected velocity profiles resemble the simulation results of Fig. 7. The PIV measurement underestimates the velocity gradient inside the expansion. Furthermore, the measurement displays a region of increased velocity just before the expansion, which largely disappears after the measurement has been corrected using the BOS data. At $s=2.5 \text{ mm}$ the velocity error is -6.5 m/s (0.15 pixel particle displacement). Compared to the simulation, the velocity error is smaller but scales reasonably well with the velocity V_s .

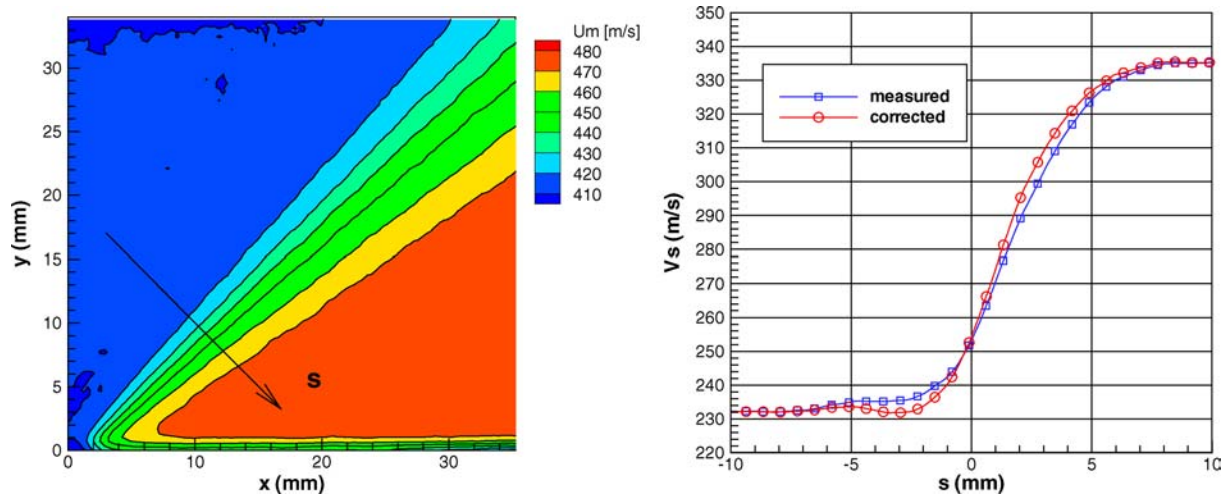


Fig. 10 Measured u -component of velocity in the expansion located at the shoulder of the 2D wedge-plate model (*left*), and profiles of the measured and corrected flow velocity V_s (*right*)

6 Conclusions

Three types of aero-optical distortion affecting PIV measurements in optically inhomogeneous media were identified. The position and velocity errors are directly related to the overall systematic error on the velocity measurement and are caused by the gradient and the second derivative of the refractive index, respectively. The particle image blur, which is related to the second derivative of the refractive index, introduces a correlation peak broadening with consequent drop in the signal to noise ratio.

Evidence of these forms of optical distortion was presented by means of PIV recordings obtained in 2D supersonic flows. Moreover, the effects were quantified with a numerical simulation of particle motion, illumination and imaging through compressible flow. Two basic flow geometries were used for the simulation: a shear layer and a 1D expansion. The assessment demonstrated that the second derivative of the refractive index in the direction of the velocity vector is the major source for the velocity error. The position error was generally of the order of 2 pixels, which is difficult to appreciate on the scale of the complete field of view. Moreover it is concluded that investigating shearing interfaces is much less critical in comparison with compression/expansion fronts. The experimental assessment of a shear layer and a Prandtl–Meyer expansion flow in a supersonic wind tunnel confirmed the results of the simulation. Furthermore, scaling rules are derived in the [Appendix](#), which indicate that PIV applications in large-scale compressible flows could suffer from serious optical distortion errors in the velocity measurement.

A verification/correction procedure for the position and velocity error was shown to be possible for 2D flows. The distortion effects due to the refractive index field were measured independently with BOS and

applied to correct the PIV measurement. Based on the results from the simulated experiments, the BOS correction reduced the velocity error almost entirely (up to 95%).

Since both the velocity error and particle image blur are related to the second derivative of the refractive index field, it is expected that the analysis of particle image blur can be used to provide quantitative information on the velocity error related to aero-optical distortion. In that case BOS measurements and 2D flow assumption will not be necessary, which deserves further attention and research.

Acknowledgements This work is supported by the Dutch Technology Foundation STW under the ‘VIDI Vernieuwingsimpuls’ program Grant DLR.6198.

Appendix

Scaling rules for high-speed industrial experimental facilities

Equation 2 indicates that the optical displacement vector, hence the error in the position of a particle, increases with W^2 (Z_D and integration length S being proportional to W). Therefore, the problem of optical distortion increases rapidly with the linear dimension (L) of the wind tunnel test section. Note that going from a small-scale research wind tunnel ($L \sim 0.1$ m) to industrial scale facilities ($L \sim 1$ m) commonly involves a scale factor for L^2 , hence W^2 , on the order of 100. However, the model dimensions and the flow features associated with the inviscid flow behaviour generally scale linearly with the wind tunnel size as well. As a consequence, the field of view is also linearly increased. Viscous flow features are expected to scale less than linear, with $L^{0.5}$ for laminar flow and approximately $L^{0.8}$ for turbulent flow (White 1991). Therefore it is expected that ∇n decreases with $L^{-0.5}$ or $L^{-0.8}$ (for a prescribed free stream density level) and that $\nabla^2 n$ hence decreases with L^{-1} or $L^{-1.6}$ for

laminar and turbulent flow, respectively. In conclusion, it is estimated that in dimensional units the position error (Eq. 2) scales at most as $L^{1.5}$, or in pixel units as $L^{0.5}$. The direct velocity error (Eq. 6) scales at most as L in dimensional units.

At optical interfaces, i.e. shock waves, the refractive index is discontinuous (its derivatives vary strongly with \vec{x}) and therefore Eqs. 2 and 6 no longer hold. In the vicinity of the interface, strong particle image blur is expected accompanied by a significant velocity error. The extent for the particle image blur scales as W , hence L , as is shown by Eq. 10. In pixel units the enlargement is independent of L .

References

- Abart JC, Molton P, Maury B, Jacquin L (2004) Implantation de la PIV dans la soufflerie transsonique S3Ch. 9th congrès franco-phonie de vélocimétrie laser, Brussels, Belgium, paper K.2
- Elsinga GE, van Oudheusden BW, Scarano F, Watt DW (2004a) Assessment and application of quantitative schlieren methods: calibrated color schlieren and background oriented schlieren. *Exp Fluids* 36:309–325
- Elsinga GE, van Oudheusden BW, Scarano F (2004b) Evaluation of aero-optical distortion effects in PIV. In: 12th international symposium on application of laser technology to fluid mechanics, Lisbon, Portugal, paper 24.4
- Haertig J, Havermann M, Rey C, George A (2002) Particle image velocimetry in Mach 3.5 and 4.5 shock-tunnel flows. *AIAA J* 40:1056–1060
- Klinge F, Riethmuller ML (2002) Local density information obtained by means of the background oriented schlieren (BOS) method. In: 11th international symposium on application of laser technology to fluid mechanics, Lisbon, Portugal, paper 15.3
- Raffel M, Kost F (1998) Investigation of aerodynamic effects of coolant ejection at the trailing edge of a turbine blade model by PIV and pressure measurements. *Exp Fluids* 24:447–461
- Raffel M, Richard H, Meier GEA (2000) On the applicability of background oriented optical tomography for large-scale aerodynamic investigations. *Exp Fluids* 28:477–481
- Richard H, Raffel M (2001) Principle and applications of the background oriented schlieren (BOS) method. *Meas Sci Technol* 12:1576–1585
- Scarano F, Riethmuller ML (2000) Advances in iterative multigrid PIV image processing. *Exp Fluids* 29, S051
- Scarano F, van Oudheusden BW (2003) Planar velocity measurements of a two-dimensional compressible wake. *Exp Fluids* 34:430–441
- Sourgen F, Haertig J, Rey C (2004) Comparison between background oriented schlieren measurements (BOS) and numerical simulations. In: 24th AIAA aerodynamic measurement technology and ground testing conference, Portland OR, USA, paper AIAA 2004-2602
- Urban WD, Mungal MG (2001) Planar velocity measurements in compressible mixing layers. *J Fluid Mech* 431:189–222
- Watt DW, Donker Duyvis FJ, van Oudheusden BW, Bannink WJ (2000) Calibrated schlieren and incomplete Abel inversion for the study of axisymmetric wind tunnel flows. In: 9th international symposium on flow visualization, Edinburgh, Scotland
- White FM (1991) *Viscous fluid flow*. McGraw-Hill, New York